aerospace

MDPI

Article

OSIRIS4CubeSat—The World's Smallest Commercially Available Laser Communication Terminal

Benjamin Rödiger [1,*], Christian Roubal [1], Fabian Rein [1], René Rüddenklau [1], Anil Morab Vishwanath [1,2] and Christopher Schmidt [1]

[1] Optical Satellite Links, Institute of Communications and Navigation, German Aerospace Center (DLR), Münchener Str. 20, 82234 Weßling, Germany; christian.roubal@dlr.de (C.R.); fabian.rein@dlr.de (F.R.); rene.rueddenklau@dlr.de (R.R.); christopher.schmidt@dlr.de (C.S.)

[2] Airbus Defence and Space, Willy-Messerschmitt-Str. 1, 82024 Taufkirchen, Germany

* Correspondence: benjamin.roediger@dlr.de; Tel.: +498153282944

Abstract

The New Space movement led to an exponential increase in the number of the smallest satellites in orbit in the last two decades. The number of required communication channels increased with that as well and revealed the limitations of classical radio frequency channels. Free-space optical communication overcomes these challenges and has been successfully demonstrated, with operational systems in orbit on large and small satellites. The next step is to miniaturize the technology of laser communication to make it usable on CubeSats. Thus, the German Aerospace Center (DLR) developed, together with Tesat-Spacecom GmbH & Co. KG in Backnang, Germany, a highly miniaturized and power-efficient laser terminal, which is based on a potential customer's use case. OSIRIS4CubeSat uses a new patented design that combines electronics and optomechanics into a single system architecture to achieve a high compactness following the CubeSat standard. Interfaces and software protocols that follow established standards allowed for an easy transition to the industry for a commercial mass market. The successful demonstration of OSIRIS4CubeSat during the PIXL-1 mission proved its capabilities and the advantages of free-space optical communication in the final environment. This paper gives an overview of the system architecture and the development of the single subsystems. The system's capabilities are verified by the already published in-orbit demonstration results.

Keywords: laser communications; satellite communications; CubeSats; New Space; miniaturization; global connectivity

Academic Editors: Davide Ferretto and Fabrizio Stesina

Received: 30 May 2025
Revised: 27 June 2025
Accepted: 1 July 2025
Published: 23 July 2025

Citation: Rödiger, B.; Roubal, C.; Rein, F.; Rüddenklau, R.; Vishwanath, A.M.; Schmidt, C. OSIRIS4CubeSat—The World's Smallest Commercially Available Laser Communication Terminal. *Aerospace* **2025**, *12*, 655. https://doi.org/10.3390/aerospace12080655

Copyright: © 2025 by the authors. Submitted for possible open access publication under the terms and conditions of the Creative Commons Attribution (CC BY) license (https://creativecommons.org/licenses/by/4.0/).

1. Introduction

Free-space optical communication (FSOC) is on the way to extend and partly replace classical radio frequency (RF) communication on satellites with a high data rate and resilient transmission channels. Small satellites and CubeSats have made their way out of academia onto the commercial market and have built up customer services. Thus, the necessity of transferring large amounts of data and having resilient channels of robust communication also increases on the smallest platforms [1]. The high data rates and the robustness against electromagnetic disturbances motivated the development of laser communication terminals (LCT) for CubeSats in the last years. The usability of FSOC in space has already been proven on large and small satellites. Tesat-Spacecom GmbH & Co.

KG (Tesat) has operated its large LCTs, with a weight of multiple tons, in the European Data Relay System (EDRS) for over two decades on large satellites [2]. SpaceX uses laser communication terminals in their Starlink constellation for inter-satellite links [3]. Smaller LCTs have been successfully demonstrated on small satellites like the Flying Laptop from the University of Stuttgart [4] and the Space Optical Communications Research Advanced Technology Satellite (SOCRATES) [5]. LCTs on CubeSats are very rare; only a few have been successfully demonstrated.

These terminals have been demonstrated using either preloaded or test data, like pseudo-random bit sequences (PRBS), and were not intended to become a commercial product. The CubeSat Laser Infrared Crosslink (CLICK) mission demonstrated a successful optical connection to an optical ground station (OGS) but could not successfully transfer data [6,7]. AAC Hyperion, together with the Netherlands Organization for Applied Scientific Research (TNO), demonstrated successful transmission of a PRBS signal using CubeCAT [8]. The National Aeronautics and Space Administration (NASA) transmitted data with the Terabyte Infrared Delivery (TBIRD) terminal at a rate of 200 gigabits per second (Gbps) [9]. Nevertheless, there was no operational interface on board that could handle these high data throughputs so that previously loaded files were transmitted [10].

The technology had to fulfill several boundary conditions to bring FSOC onto the commercial CubeSat market and into mass production. The LCT had to reach a level of compactness and efficiency so that it could be integrated into a standard CubeSat, allowing for an easy and simple integration. Using standardized platforms also required standard interfaces and compatibility with existing infrastructures. Thus, the German Aerospace Center (DLR) and Tesat set the goal of developing a highly miniaturized LCT, especially designed for CubeSats, to meet a customer's use case requirements.

The outcome was the development of the Optical Space Infrared Downlink System (OSIRIS) program, developed as the terminal OSIRIS4CubeSat, the world's smallest LCT measuring only one-third of a CubeSat unit in size, with a mass of 395 g, and with a data rate of 2 to 100 megabits per second (Mbps). With a power consumption of a maximum of 8.5 W, it surpasses the capabilities of most CubeSat RF transmitters in terms of power-per-bit and volume-per-bit ratios. The intention of the development was—besides the successful in-orbit demonstration—to commercialize the terminal as a product under the name CubeLCT by Tesat [11]. OSIRIS4CubeSat, at the time, was developed and demonstrated the first LCT, which had the form factor to fit in a CubeSat and was able to transmit operational data. Thus, it can be said that OSIRIS4CubeSat was the first laser terminal prepared for a commercial market. This publication focuses on the design decisions and the development of the technology of the single subsystems and the entire terminal. Even though the strong focus of this publication is on the technology of the terminal, a brief summary of the in-orbit demonstration is given at the end.

2. Concept of Laser Communication on CubeSats

While CubeSats have a long list of advantages like low cost and quick access to space, they are very limited regarding size, weight, and power (SWaP) of the satellite and the payloads. Classical CubeSats have dimensions of 10 × 10 × 10 cm (called one unit, U) and consist of one or multiple units. The outer shell of the CubeSat is covered with solar cells that provide power to the satellite bus and payloads. Starting as students' experiments in academic education, CubeSats made their way into scientific and commercial missions with increasing demands for data rates between spacecraft and the ground segment [12].

Therefore, the concept of a laser communication terminal on a CubeSat was to enable the highest possible data rate within the boundary condition of limited SWaP. The advantage of optical communication over traditional RF links derives from a smaller

divergence angle and, thus, higher power density on the ground—but this also comes with the disadvantage of guiding the highly directed laser signal from the satellite to the ground. To reduce power consumption, OSIRIS4CubeSat was designed to be in the sweet spot between the low divergence of the laser beam and the pointing capabilities of the satellite. Due to the limitations of CubeSats, the attitude determination and control system (ADCS) had a limited performance in the range of 1° at the start of the development. Therefore, the terminal is equipped with a fast-steering mirror (FSM) as a fine pointer in the range of ±1°, while the satellite's ADCS is used for coarse pointing into the range of the FSM. Since the design and manufacturing of the CubeSat were outsourced, all necessary control design considerations concerning the body pointing accuracy and orbit perturbations were handled by the satellite manufacturer.

To reduce the size and weight of the payload, it is necessary to look at the design of OSIRIS version 1 and 2 (OSIRISv1 [4, 13] and OSIRISv2 [14]) for satellites in the 100 kg class. The electronics are separated from the optics and connected via fibers. To miniaturize the payload, the development is based on a patented solution [15] that combines electronics and optical components on one printed circuit board (PCB) that acts as an optical bench as well as a classical PCB. Therefore, no additional optical bench is needed, and the electrical components are mounted in the gaps between the optical components. The design is optimized in a way that the PCB is stiff enough to act as an optical bench and still fulfills the electrical requirements and demand in terms of thermal behavior [16].

The pointing, acquisition, and tracking (PAT) followed the verified approach that has been used in many aircraft downlinks as well as on the Bi-spectral Infrared Optical System (BiROS) and Flying Laptop satellites. Therefore, the OGS is equipped with a beacon laser pointing towards the satellite. The FSM of the laser terminal drives a search spiral and stops as soon as the signal from the ground is detected on the tracking sensor. A four-quadrant diode (4QD) is an established technology, used in the previously mentioned projects, and is therefore used as an acquisition and tracking sensor in OSIRIS4CubeSat as well. Both the OGS and laser terminal compensate the dynamics in the link via a two-axis control loop with the telescope and FSM [17].

From the beginning of the development, the goal was to develop a laser communication terminal for a market application and not only for one dedicated flight. Therefore, the goal was to use standard interfaces wherever possible to remain compatible with different CubeSat platforms. Also, for the space-to-ground interface, a standardized approach was followed using the Consultative Committee for Space Data Systems (CCSDS) optical on–off-keying (O3K) standard for compatibility between the laser terminal and the ground segment.

3. Terminal Hardware Design

The patented design of using the PCB as the optical bench enabled the high miniaturization factor of OSIRIS4CubeSat. Furthermore, the very compact design ensured that all subsystems of optics, mechanics, electronics, and major parts of the software were combined into one device. The software was distributed over these subsystems, and parts were even outsourced to the satellite bus. Hence, the software—as its own system—is described below in Chapter 4. On a conceptual level, optics and mechanics are handled as one single subsystem, the optomechanics. Thus, optomechanics and electronics are explored in further detail in the following sections.

The terminal was developed according to the PC/104 standard, which is commonly used by several CubeSats manufacturers. The mechanical layout of OSIRIS4CubeSat is based on this standard. For an efficient and compact design, the LCT does not use the relatively large 104-pin connector but uses small standard interfaces to increase

compactness. The terminal uses completely passive cooling during the non-operating phases. The terminal can be viewed in Figure 1.

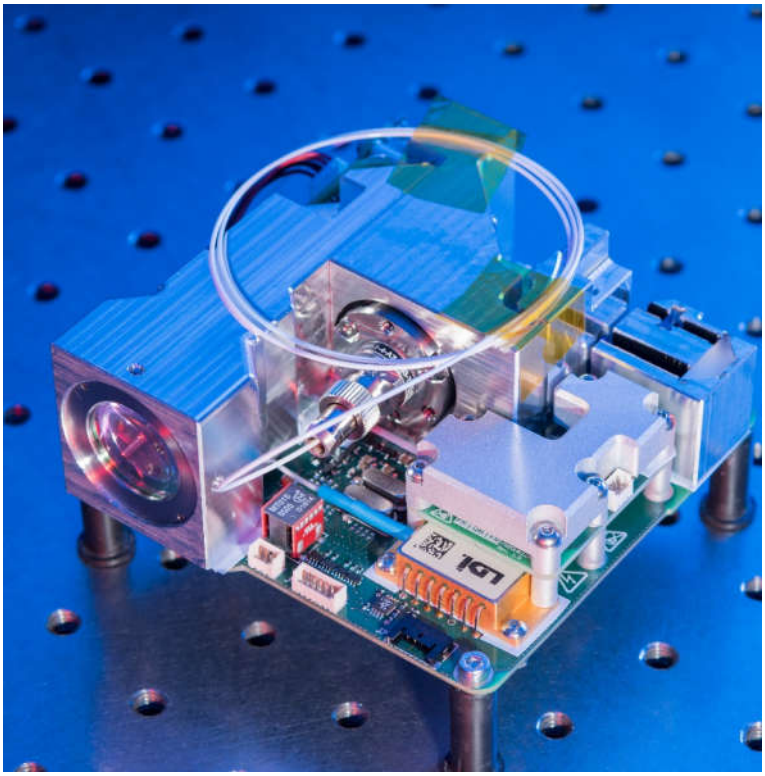

Figure 1. Flight model of the OSIRIS4CubeSat LCT [18].

The LCT, displayed in Figure 1, performs the PAT, generates the transmission laser, and modulates it with the data to send. Therefore, it is equipped with a microcontroller as a processing unit that controls the PAT, laser power, and thermal behavior of the transmitter laser. The preparation of the transmission data, e.g., the channel coding and the high sampling of the terminal telemetry for scientific evaluation, require a high amount of processing power, which overcomes the abilities of a microcontroller. Thus, these software parts have to be processed on other subsystems of the satellite.

3.1. Link Budget

The base for the development of the terminal is the theoretical calculation of the feasibility of link establishment. Therefore, a link budget was calculated. The basic parameters for the link budget are based on the targeted operation's environment of the terminal. The terminal was designed for use in low earth orbit (LEO), so an orbit height of 500 km was assumed for the link budget. Two link budgets had to be calculated, one for the tracking in the uplink direction and one for the data transmission in the downlink direction. The terminal separated up- and downlink by wavelength, with 1590 nm for the uplink and 1550 nm for the downlink. The link budget was calculated for the maximum data rate of the terminal of 100 Mbps. As the counterpart on the ground, the parameters of DLR's OGS were considered as a receiver.

The link margin LM of an optical link can be calculated similarly to a link margin for RF links with

$$\mathrm{LM} = \mathrm{P_{Tx}} - \mathrm{L_{Tx}} + \mathrm{G_{Tx}} - \mathrm{L_{jit}} - \mathrm{L_{dist}} - \mathrm{L_{atm}} - \mathrm{L_{sci}} + \mathrm{G_{Rx}} - \mathrm{L_{Rx}} - \mathrm{P_{sens}} \quad (1)$$

where the single terms are described in the following paragraphs. A link margin of 3 dB had to be reached in both directions as the minimum requirement for the terminal's design consideration.

Transmitter power: In the uplink direction, two erbium-doped fiber amplifiers (EDFA) were used to generate the beacons for the PAT. Each EDFA emitted light at 4 W, which led to

$$P_{Tx} = 8\ W \tag{2}$$

for the uplink. Power and space are very limited on a CubeSat. The compact and efficient design of OSIRIS4CubeSat required a compact laser source. Thus, a high-power laser diode (HPLD) was used instead of a fiber amplifier. The HPLD generated an optical output power with

$$P_{Tx} = 100\ mW \tag{3}$$

at the fiber output.

Transmitter loss: The beacons were modulated with a 10 kHz sine to distinguish the beacons from reflections and background light. Further losses are usually negligible, but 1 dB was added as an additional margin, which led to a total loss of

$$L_{Tx} = 1\ dB + 1.95\ dB = 2.95\ dB. \tag{4}$$

The optical output power of 100 mW was measured at the end of the pigtailed fiber of the HPLD. The optical system of the terminal caused losses due to absorptions and truncations. The losses were measured at 35%, or

$$L_{Tx} = 1.87\ dB. \tag{5}$$

Transmitter gain: Antenna gain for optical transmitters can be calculated similarly to RF antennas by comparing the area depending divergence with an isotropic radiator. The collimators of the OGS beacon system had a divergence of 0.573 mrad (full angle, 1/e2), which led to an antenna gain of

$$G_{Tx} = 10\,log_{10}\left(\frac{A_{iso}}{A_{LCT}}\right) = 81.49\ dB. \tag{6}$$

OSIRIS4CubeSat was intended to be diffraction-limited, which led, with an aperture of 20 mm, to a divergence of 0.193 mrad (full angle, $1/e^2$). During the integration, the real divergence measured 0.203 mrad (full angle, $1/e^2$). This led to an antenna gain of

$$G_{Tx} = 10\,log_{10}\left(\frac{A_{iso}}{A_{LCT}}\right) = 90.50\ dB. \tag{7}$$

Jitter loss: The jitter loss of the OGS could be measured using several orbiting objects. The losses are negligible but were considered as an additional margin with

$$L_{jit} = 1\ dB. \tag{8}$$

The loss caused by the LCT's fine pointing system is highly dependent on the tracking capabilities, which depend on atmospheric effects. As these effects were unknown before the mission, a conservative margin of

$$L_{jit} = 3\ dB \tag{9}$$

was taken into account.

Distance loss: The main contribution to the link budget is geometrical loss due to the distance between the satellite and the OGS. The link budget considers a successful connection above 10° elevation, which led to a distance of 1815.4 km. The resulting loss was

$$L_{dist} = \left(\frac{4\pi d}{\lambda_{uplink}}\right)^2 \triangleq 20\log_{10}\left(\frac{4\pi \cdot 1815.4\ \text{km}}{1590\ \text{nm}}\right) = 263.14\ \text{dB} \quad (10)$$

for the uplink and

$$L_{dist} = \left(\frac{4\pi d}{\lambda_{downlink}}\right)^2 \triangleq 20\log_{10}\left(\frac{4\pi \cdot 1815.4\ km}{1550\ nm}\right) = 263.36\ \text{dB} \quad (11)$$

for the downlink.

Atmospheric loss: To calculate atmospheric loss, models to describe the atmosphere's behavior have to be used. No specific model for the atmosphere around the OGS at DLR exists [19]. Worst-case parameters would have been too pessimistic and would have set too strict requirements for the terminal's design. Thus, a transmission fraction () of 0.92 was selected as a reasonable value for the atmosphere around DLR's OGS, based on previous experiment experiences. This led to the atmospheric loss of

$$L_{atm} = 10\log_{10} T_z^{\,1/\sin(\varepsilon)} = 2.91\ \text{dB} \quad (12)$$

in both directions.

Scintillation loss: Scintillation loss is caused by turbulence in the atmosphere. In the far field, a simplification of the power scintillation index (PSI) can be used for link budgets, which is equal to a normalized scintillation index (σ_P^2). The calculations, according to [20] (pp. 46–58), led to a PSI of 0.525. Due to short integration times, a loss fraction (p_{thr}) of 0.1 was considered, which led to a scintillation loss of

$$L_{sci} = -4.342\left\{\text{erf}^{-1}(2p_{thr} - 1)\cdot\sqrt{2\ln(\sigma_P^2 + 1)} - \frac{1}{2}\ln(\sigma_P^2 + 1)\right\} = 4.53\ \text{dB}. \quad (13)$$

The scintillation index in the downlink direction was measured during several campaigns with the considered OGS and other LCTs [21]. Thus, a PSI of 0.166 was chosen, which covered 80% of all analyzed experiments. With a loss fraction of 0.01 (as a consequence of the chosen error correction schemes, which are explained later in Chapter 4), the scintillation loss in the downlink direction was calculated to

$$L_{sci} = -4.342\left\{\text{erf}^{-1}(2p_{thr} - 1)\cdot\sqrt{2\ln(\sigma_P^2 + 1)} - \frac{1}{2}\ln(\sigma_P^2 + 1)\right\} = 4.29\ \text{dB}. \quad (14)$$

Receiver gain: The first lens of the LCT could be interpreted as the effective receiving antenna surface. A radius of 10 mm led to a receiver gain of

$$G_{Rx} = 10\log_{10}\frac{4\pi \cdot A_{O4C}}{\lambda_{Uplink}^2} = 91.94\ \text{dB}. \quad (15)$$

DLR's OGS has a primary mirror (M1) with a radius of 30 cm and a secondary mirror (M2) with a radius of 14.14 cm. The surface area of M2 has to be subtracted from the area of M1, which led to a receiver gain of the OGS of

$$G_{Rx} = 10\log_{10}\frac{4\pi \cdot (A_{M1} - A_{M2})}{\lambda_{Downlink}^2} = 120.61\ \text{dB}. \quad (16)$$

Receiver loss: The optical properties of each optical element of OSIRIS4CubeSat could be characterized very well during the integration. It turned out that the losses are less than 80%, which leads to a consideration for the link budget of

$$L_{Rx} = 0.97\ \text{dB}. \quad (17)$$

Also, the optical losses inside the OGS were very well known and measured. They are given by

$$L_{Rx} = 0.46\ \text{dB}. \quad (18)$$

Receiver sensitivity: The sensitivity of both receivers was characterized in the laboratory before integration and can be included in the link budget. They result in

$$P_{sens} = -67.05 \text{ dBm} \quad (19)$$

in the uplink direction and

$$P_{sens} = -48.92 \text{ dBm} \quad (20)$$

in the downlink direction.

A summary of the link budget can be found below in Table 1.

Table 1. Link budget of OSIRIS4CubeSat.

Parameter	Uplink (1590 nm)	Downlink (1550 nm)
P_{Tx}	39.03 dBm	20 dBm
$-L_{Tx}$	−2.95 dB	−1.87 dB
$+G_{Tx}$	81.49 dB	90.5 dB
$-L_{jit}$	−1 dB	−3 dB
$-L_{dist}$	−263.14 dB	−263.36 dB
$-L_{atm}$	−2.91 dB	−2.91 dB
$-L_{sci}$	−4.53 dB	−4.29 dB
$+G_{Rx}$	91.94 dB	120.61 dB
$-L_{Rx}$	−0.97 dB	−0.46 dB
P_{sens}	−67.05 dBm	−48.92 dBm
LM	4.01 dB	4.14 dB

The positive link margin showed that the design and the concept are feasible to fulfill the requirements to establish an optical connection in a 500 km orbit above 10° elevation. It has to be mentioned that no coding gain was considered in the link budget as it was already sufficiently positive.

3.2. Optomechanics

The goal of OSIRIS4CubeSat to be compact and power-efficient and to provide a downlink data rate of 100 Mbit/s led to the requirements of a narrow beam divergence and active beam steering. A commercial off-the-shelf (COTS) FSM with a mirror size of 4.6 mm was used in combination with a 4QD for closed-loop tracking of a beacon sent from an OGS. The beam divergence was larger than the maximum expected point ahead angle (PAA) of ~50 µrad [22] for the satellite LEO so that the beam still hits the OGS while tracking on the beacon. This induces additional pointing loss but reduces the overall system complexity since no second steering mirror for compensation of the PAA is needed. The optical output power of the laser, minimum beam divergence, and available mirror sizes constrained the optical system's clear aperture. Thus, the beam diameter must be less than 2 mm for the tracking system and the demand for a telescope to expand the transmitter beam.

Figure 2 shows a ray trace model of the optical system, with green and cyan rays indicating the optical path of the transmitter (Tx) subsystem at 0° and 1° field angles and with blue and magenta rays indicating the optical path of the receiver (Rx) subsystem at 0° and 1° field angles. The optical signal of the laser is coupled from a single-mode fiber into free space by a collimator, reflected by a dichroic beam splitter (DBS), reflected by the FSM, and then expanded by the Keplerian telescope with a magnification of 7.2, leading to a $1/e^2$ beam diameter of 10.2 mm at the output aperture.

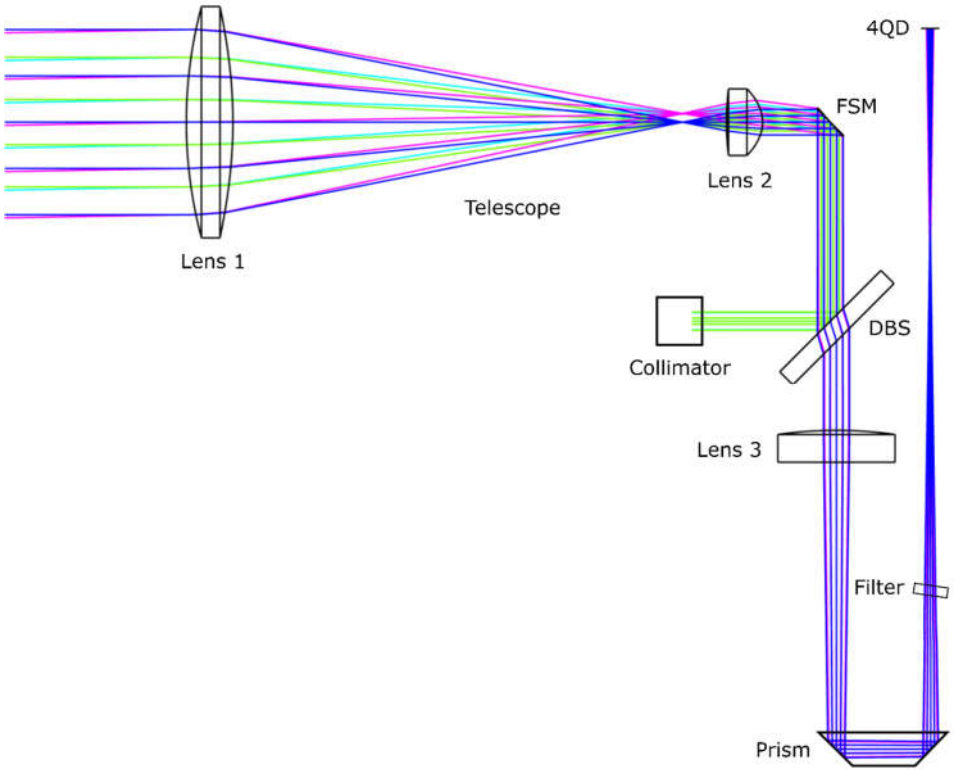

Figure 2. Ray trace of the optical system. Transmitter (Tx) subsystems are indicated by green (0°) and cyan (1°), and receiver (Rx) subsystems are indicated by blue (0°) and magenta (1°) rays.

In the Rx direction, incoming light is collected with Lens 1 and collimated at a reduced beam diameter with Lens 2 in the telescope. The FSM is located at the pupil position to minimize lateral beam offsets in the optical system. The beam is transmitted through the DBS and projected onto the 4QD by Lens 3. Between Lens 3 and the 4QD, a dove prism folds the optical path and a notch filter suppresses stray light coming from the laser source itself and from outside of the terminal. Where possible, COTS components were used, as in, for example, the FSM, collimator, and Lens 3.

Since no COTS optics were available for the telescope, a custom design was made with two aspheric lenses optimized on minimal wavefront error over a field of regard (FOR) of ±1°. This also minimized the divergence for off-axis Tx beams while keeping a symmetric beam shape at the 4QD for the tracking system.

The concept of the optical system design relied on a precise alignment between the Tx and Rx systems, as no coarse pointing system was used. The angular offset between the two systems needed to be kept below 30 µrad to minimize resulting power losses and fulfill the link budget. In addition to that, the assembly and adjustment must be time efficient. Therefore, the mechanical structure was based on two aluminum blocks joint together with screws and alignment pins to provide a basis for the optical system and mainboard PCB. The terminal itself was fixed to the satellite structure via four holes in the mainboard so that the optomechanical system was not directly coupled to the satellite frame structure. This prevented optical misalignment due to stress-induced bending. For the same reason, optical components for the tracking system were mounted inside one solid block. The DBS, prism, and filter were made of N-BK7 and glued directly to the aluminum block. During the gluing process, the DBS and prism were pushed against precisely machined reference surfaces. Lenses 1–3 were also made of N-BK7 and mounted into titanium cells for an optimized coefficient of thermal expansion (CTE) match to minimize stress-induced wavefront error and risk of mechanical damage.

The collimator divergence was adjusted for wavefront error by using a shearing interferometer and a camera. After integration of all other optical elements, the telescope's divergence was adjusted by rotating the aperture lens cell in its fine pitched thread. For minimizing the wavefront error, a shearing interferometer and a camera were used as well. The second-last step was the angular alignment of the Tx and Rx systems. As the Rx system was fixed in position, the only degree of freedom was a tilt control of the collimator tumbling plate. This did not change the position of the integrated collimator lens, as the whole assembly of the fiber connector, tumbling plate, and lens were tilted against its mounting structure. A residual angular offset between the Tx and Rx systems of less than 3 µrad was achieved and maintained after qualification tests. Due to the increased difference in refractive index between the glass material and vacuum compared to that in the air, focal lengths of the lenses decreased and would have led to a higher divergence for the Tx system and a change in the beam size at the 4QD. A simulation showed that it was sufficient to compensate for the change in focal length with the aperture lens of the telescope.

3.3. Electronics

A detailed overview of the electronics is given in [23]. The electronic system of the payload was mainly integrated on one PCB, which—as already described—also served as the carrier board for the optomechanical system. This allowed for not only a very compact design but also for short interfaces to the optical sensors and actuators within the optical path.

CubeSats have limited space and power resources. For this reason, it was important to design a power-efficient small transmitter system that was not too complex and was easy to control. In this development, an HPLD was used, and more complex systems such as EDFAs, which are usually used for high-power/high-data-rate optical systems, could be avoided.

As shown in Figure 3, the HPLD circuit featured a power monitoring output and an adjustable current source (I_{SET}) for current adjustment. This was used for optical power control in the microcontroller. Additionally, an integrated thermoelectric cooler (TEC) using a temperature control circuit with a switched output stage was integrated into the PCB to keep the temperature of the HPLD stable during operation.

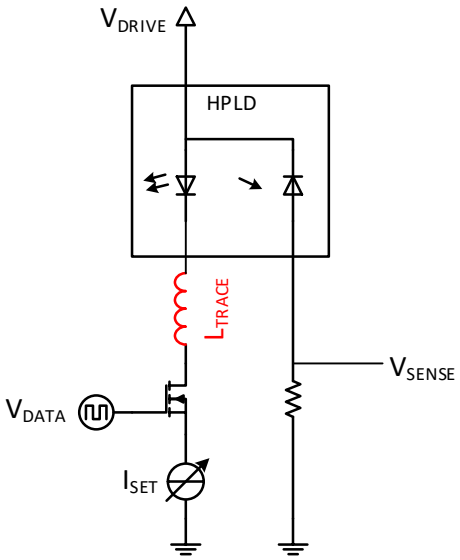

Figure 3. HPLD driver circuit (simplified).

The approach of using an HPLD made it difficult to achieve a high output power and high data rate at the same time. It was necessary to reduce parasitic inductivities (L_{TRACE}) to a minimum, but this was limited by the physical dimensions of the butterfly package. To further increase the rise time and therefore achieve the required data rate of 100 Mbps, the driver used an increased supply voltage (V_{DRIVE}) and additional compensation.

The optical signal integrity is shown in Figure 4. It demonstrates that the overshoot was one sided and at ~10%. The power consumption of the transmitter circuit was 6.15 W (without TEC) at 103 mW optical output power and 100 Mbps. This fulfilled the requirements of the terminal to generate a reliable optical data transmission signal that matches the link budget.

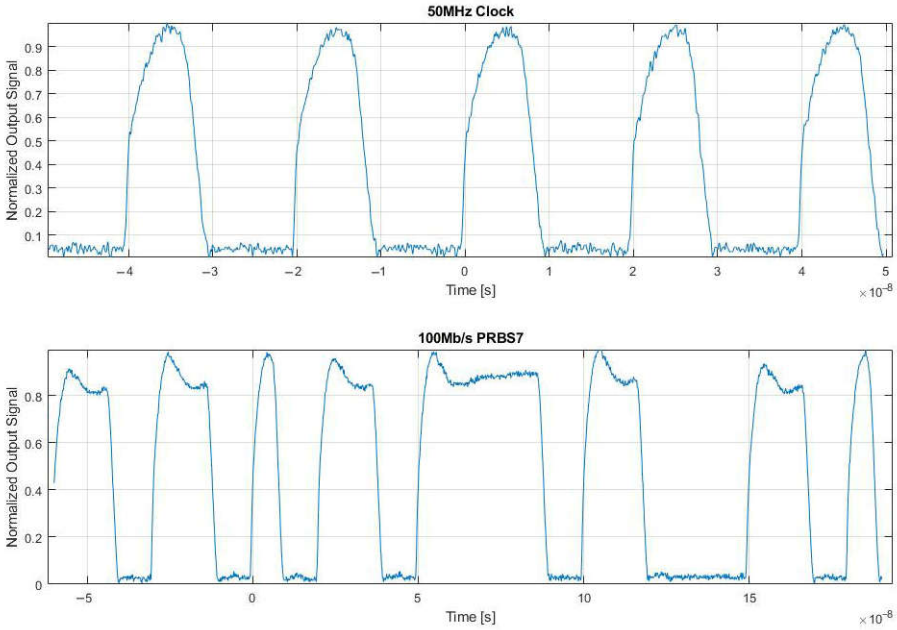

Figure 4. HPLD output signal.

4. Software Concept

The software in OSIRIS4CubeSat was mainly developed on two subsystems, the terminal microcontroller (MSP430f1611) and the NanoCom software-defined radio (SDR), a zynq7000 field programmable gate array (FPGA) from Xilinx with a dual-core ARM Cortex A9 processor. The terminal firmware was responsible for managing the electronic system inside the optical terminal and for executing and controlling the PAT control loop. The software modules in the NanoCom SDR were responsible for overall configuration and management of the optical terminal, data management, telecommand, and telemetry operations. The distribution and separation of the different software parts is illustrated in Figure 5.

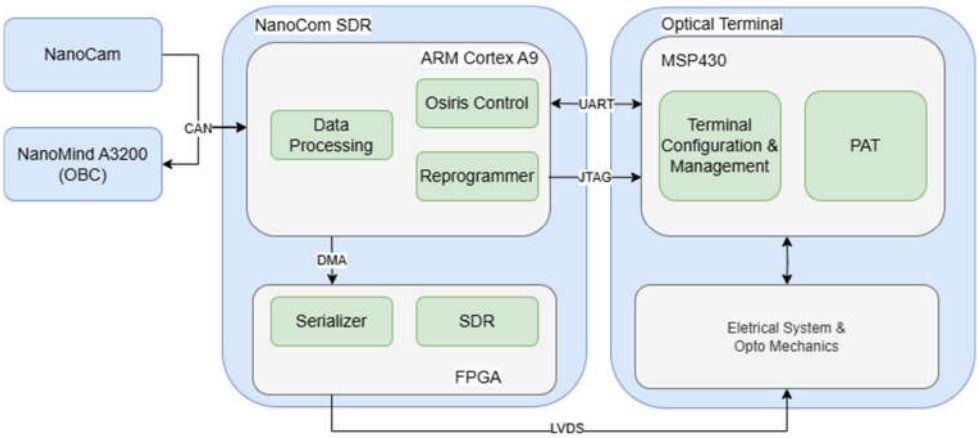

Figure 5. Software components in OSIRIS4CubeSat.

4.1. Terminal Firmware

The terminal firmware configured and managed the electronic components of the transmitter system described in Section 3.2. and the control loop of the PAT described below in Section 4.2. The microcontroller MSP430 had two universal synchronous/asynchronous receiver/transmitter (USART) interfaces, where one of those was configured as a serial peripheral interface (SPI) for communicating with the FSM driver. The second USART was configured as a UART for communicating with the control software on the NanoCom SDR. Two clock sources were available, an 8 MHz quartz crystal and a backup 16 MHz temperature-compensated crystal oscillator (TCXO). An analog-to-digital converter (ADC) was configured to sample the voltage levels from the 4QD. Additionally, a joint test action group (JTAG) interface was also foreseen for software updates in orbit.

On powering up, the MSP430 configured its above-mentioned peripherals and indicated its availability to the control software on the NanoCom SDR and waited for further commands from the latter. Upon receiving a command to perform an integrity check, the firmware calculated the checksum on its program segment to detect any possible bitflips. Once the calculated checksum matched the checksum stored on the control software, the necessary configuration for the terminal operation (i.e., output laser power to be used, pattern to be executed for acquisition, etc.) were sent over the UART interface. During nominal operations, the terminal was commanded to perform the PAT.

During pointing, the terminal firmware sent appropriate digital-to-analog converter (DAC) values to the FSM driver over the SPI interface to execute a hexagonal spiral. It continued to perform this until the beacon was visible on the 4QD. Once the beacon was on the 4QD, it entered the acquisition phase where it positioned the beacon at the specified target offset. A proportional–integral (PI) controller ensured that the beacon remained at the target offset. Once the signal was lost and no signal was visible on the 4QD, it continued executing the spiral pattern from its last acquired position. The control loop was executed at 200 Hz. This process is described in Figure 6.

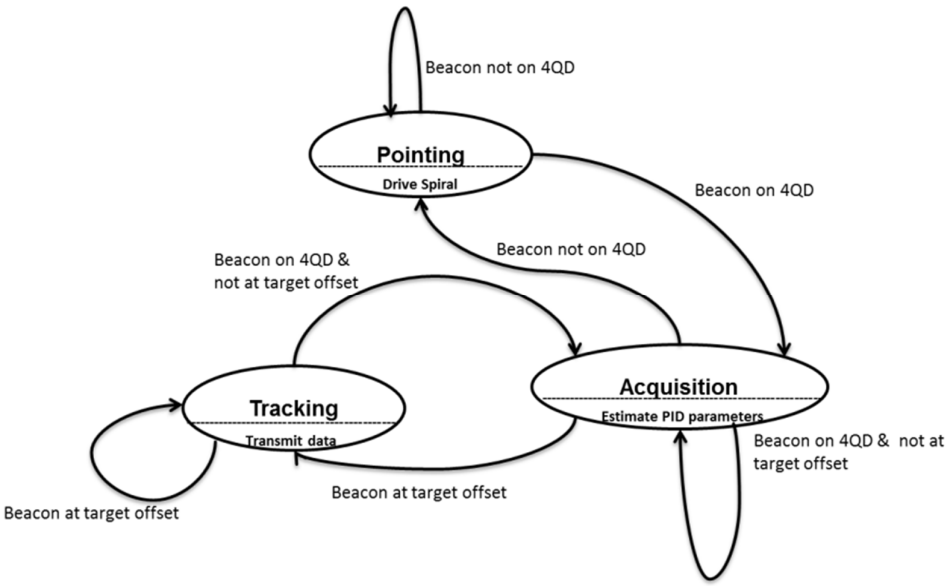

Figure 6. State diagram for pointing, acquisition, and tracking.

Additionally, the optical power control of the transmitter was also implemented as part of the terminal firmware. The microcontroller sensed the average optical power with the integrated photodiode of the HPLD and controlled the laser diode current and, with this, the output power. The implemented PI controller was optimized for robustness, as the disturbances were mainly thermal. Nonetheless, a challenging exception needed to be covered by the optical power controller: the microcontroller had no information on whether data had currently been sent or not. If no data were sent, no optical output would be generated and, therefore, the integrating behavior of the controller would have caused a high setting current for the HPLD. This would possibly have led to destruction of the diode if the data transmission began again. For this reason, the controller checked if there was any output power. If not, it checked if there should have been any output (i.e., if the setpoint differs from "0"). If this was the case, the control loop was stopped, and the optical output was set to a relatively low, but measurable, value. If the data transfer now began, control was restarted from this point.

During these procedures, the terminal firmware also sent the scientific data (telemetry sampled with a high frequency of 200 Hz), including 4QD values, FSM positions, controller values, laser output power, TEC values, error flags, etc., back to the control software over UART, which was subsequently timestamped and stored in the memory of the SDR.

4.2. PAT Control Loop

The PAT controller design and associated logic, developed for OSIRIS4CubeSat, enabled precise beacon tracking by adapting to hardware characteristics and expected disturbances by the atmosphere and platform vibrations up to a certain level [17]. It included automatic gain control that dynamically adjusted the receiver gain to maintain an optimal signal-to-noise ratio, preventing saturation while ensuring sufficient dynamic range.

The acquisition phase was critical for establishing an optical link. Since the LCT initially lacked precise beacon orientation knowledge, it relied on satellite body pointing and a predefined search pattern. A spiral search, based on an Archimedean design, ensured uniform coverage while maintaining efficiency. The increment was carefully selected to account for satellite drift, ensuring the beacon was not missed. This design

balanced the need for rapid detection with the requirement to compensate for body pointing errors. The search was limited to prevent actuator saturation, and once a valid signal was detected, the system transitioned to tracking mode.

In tracking mode, the beam steering was continuously adjusted to maintain precise alignment. The implemented PI controller balanced error minimization with stability. The FSM was modeled as a second-order system, while the tracking sensor introduced additional filtering. A low-pass filter suppressed resonance and noise, ensuring accurate signal processing. To handle signal interruptions, the system paused tracking for 50 milliseconds, enabling rapid reacquisition in case of power fades. If the signal remained lost, the search restarted from the last known position.

Another aspect of the acquisition and tracking control logic dealt with stray light caused by the internal transmitter coupling onto the tracking sensor under certain conditions. When the mirror was operating close to its maximum deflection angle, parts of the transmission beam were reflected by the optomechanics. The reflected light passed through the PCB material and increased the power on the 4QD. This led to a misinterpretation of the transmission laser as a beacon, and the terminal started tracking its own laser beam. By developing an adaptive threshold dependent on laser output power and FSM deflection angle, this additional disturbance could be mitigated by the software [24].

4.3. Channel Coding

The NanoCom SDR, together with the NanoCom TR-600, provided S-band connectivity to the mission. However, the NanoCom SDR mainly exploited the FPGA for providing this functionality, and the processor was mostly untapped. The software packages for configuration and management of the optical terminal and for data processing were therefore hosted on the processor of the NanoCom SDR. The processor was running a customized Linux OS, thereby making it lightweight and equipping it with the libraries necessary for executing the necessary functions.

The following peripherals, which we were introduced to in Figure 5, were used: UART for communicating with the terminal firmware, JTAG for reprogramming MSP430 for software updates, AXI direct memory access (DMA) for data transfers between the processor and the FPGA, and finally a controller area network (CAN) interface for communicating with other subsystems in the satellite. The three main functionalities of the software were to manage the configuration and scientific data of the optical terminal, provide software updates in orbit for terminal firmware, and prepare the data for optical downlink. Each of these functionalities are described further in this section.

4.3.1. OSIRIS Controller

The OSIRIS controller was a multi-threaded application responsible for managing the operations of the optical terminal before, during, and after the optical downlink. One of the threads was responsible for interacting with the satellite's onboard computer (OBC) over the CAN interface. The protocol for communication was the CubeSat space protocol (CSP), which was also the language spoken by the rest of the subsystems within the satellite. This thread would listen for the commands from the satellite's OBC and execute them as and when necessary. It would also relay the telemetry data from the terminal firmware to the satellite OBC to evaluate the performance of the system in real time on the ground. The second thread accomplished the task of sending the data blob through the serializer to the HPLD inside the optical terminal. The final thread performed actual configuration and management of the terminal firmware. The configuration that was used for the optical downlink was available as an xml file located at a predefined mountpoint. Any changes to the configuration of the terminal would have therefore meant adapting

this xml file or replacing it with a newer version. This thread read the configuration present in the xml and relayed it to the terminal firmware over the UART interface. It also collected the scientific data described earlier, timestamped it, and stored it in a local file. This file could have been downloaded over the classical links to the ground afterwards, enabling further insight into the performance of OSIRIS4CubeSat. In case of errors or warnings, the terminal firmware flagged these to the OSIRIS controller and appropriate actions were taken onboard.

4.3.2. Re-Programmer

Since most components selected for OSIRIS4CubeSat—including the MSP430—were COTS components and were not radiation-hardened devices, bit flips on memory units on some of these devices were expected. Hence, it must have been possible to detect and correct these errors, which can potentially cause the optical terminal to misbehave. Although MSP430 was shipped with an inbuilt bootloader that can be used to program its flash memory, if a bitflip caused by radiation was detected on the section of memory where the bootloader was stored, it would have no longer been possible to rewrite the MSP430, which would have resulted in the loss of the mission. Therefore, a more resilient approach to reprogramming the MSP430 through the JTAG interface was selected. This application was responsible for rewriting the microcontroller during such incidents. Whenever the checksum evaluated by the terminal firmware would not match the checksum stored in the xml file on the OSIRIS controller or when a newer version of the terminal firmware was uploaded onboard, this application was invoked to ensure the integrity of the firmware on the MSP430.

4.3.3. Data Processing

The main objective of the mission was to transfer pictures taken by a NanoCam to the ground using the optical link at 100 Mbps. Traditionally, in FSOC, the atmosphere plays a big role in defining the quality of the link. Strong turbulence, high wind speeds, and the presence of clouds results in bursts and/or intensity/phase fluctuations in the received optical signal that need to be compensated in order to establish effective downlinks. Therefore, it is imperative to adapt the data sent over the optical channel to overcome these effects. This application was responsible for preparing the pictures taken by the NanoCam and making them suitable for transmission to the ground. One of the effective ways to achieve error correction is by using forward error correction (FEC) in order to correct the errors in each frame through parity symbols. Hence, a Reed–Solomon (RS) encoder was employed. In case of FSOC, FEC in itself is often not sufficient, as this cannot correct the burst errors induced by the channel because of clouds, etc. Therefore, the FEC was complimented with deep channel interleavers, which could account for fades of even up to a few seconds. Having a long sequence of 1s or 0s might damage the HPLD as it might continue to integrate over time. Therefore, direct-current (DC) balancing was achieved through a scrambler. And finally, in order to effectively recover the clock on the ground, synchronization symbols were attached at the beginning of each frame. This process is described in Figure 7 below.

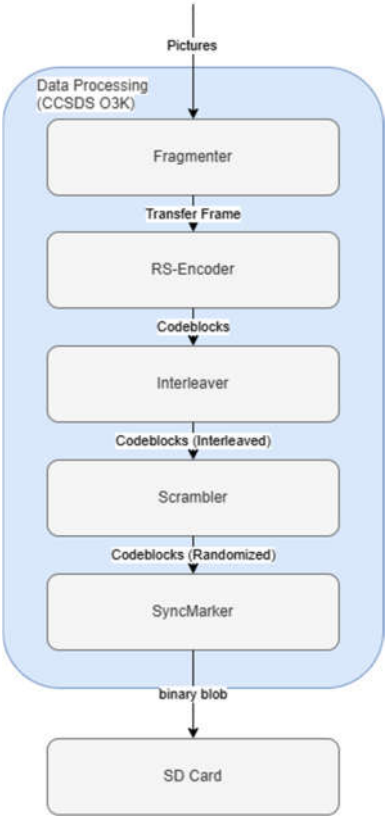

Figure 7. Data processing functions.

These data processing functions needed to be configured appropriately in order to effectively mitigate the effects of the free-space optical channel. Based on previous experiments, the channel correlation time and the power scintillation index over elevation from LEO to ground were measured [25]. The channel correlation time indicates the number of fades and the fade duration that can be expected for LEO to ground optical links. The deep interleaver was set up to overcome the worst fades measured during these experiments. When transmitting compressed images, it was noticed that the position of the errors became extremely important along with the number of errors. For example, if post-processing was carried out on the ground and an error still persisted on the Huffman table of a transmitted JPEG image, the entire image would have been rendered unusable even when the rest of the image was error-free. The lack of an optical uplink meant that the system was half-duplex, making it unfeasible for connection-oriented application protocols. Therefore, it was extremely important to provide stronger protection with RS (255, 191). The performance of the above data processing functions was evaluated during the ground tests [26] and was found to be very satisfactory. The expected optical channel for LEO-to-ground links are typically less turbulent, like it was during these tests, thereby providing a high degree of confidence in using the same configuration for the final system.

Learning from this mission was incorporated into the later published CCSDS O3K standard [27]. However, since at the time of development of this mission, this standard was not published, slight deviations (such as configurable code rates and additional synchronization symbols) can be expected. The pictures taken by the NanoCam were transferred through the CAN interface to NanoCom SDR. This application then processed all the pictures present at a predefined mountpoint according to [27] and produced a binary blob, which was later transmitted through the optical terminal to the ground. The configuration to be used for processing such as code rates, interleaver depths, and pointer

to the binary blob was available in the xml file at OSIRIS Controller. The processing was carried out offline since the throughput from the CAN interface was much slower than the necessary channel throughput for the optical interface.

The method for transmitting the pictures without the need for additional higher-layer protocols while still complying with the O3K standard was patented [28].

5. In-Orbit Demonstration

The functionalities and capabilities of OSIRIS4CubeSat were demonstrated in an operational mission on a 3U CubeSat called PIXL-1. The results of the successful payload verification and validation by an optical data transmission can be found in [29]. Besides the end-to-end transmission, the tracking behavior could also be proven. The results can be found in [17]. These two publications cover the entire acquisition process and mitigation techniques for inaccurate orbit files and discuss the performance of the PAT system. The major result was the verification of the data transmission with OSIRIS4CubeSat using the O3K standard. For example, during one connection of 116 s, 1.17 GB of data were transmitted (and received), which contained 4731 pictures, of which 2699 could be decoded completely error-free. This underlined the capabilities and performance of OSIRIS4CubeSat. Furthermore, this means that the developed FEC schemes were sufficient to correct most of the atmospheric effects.

The successful link acquisition and the stable tracking could be verified multiple times. It was possible to establish an optical connection from 5° elevation onwards (the LCT is turned on only above this elevation angle) but could be kept on below 5° elevation in the descent part of the links. The optical link budget as a base for the design and the development of the LCT considered 10° elevation as a possible starting point. It can be said that whenever the satellite pointed correctly, an optical link could be reliably established, regardless of the elevation. Even though the optical power could not be measured directly at the OGS; the results indicated that the described considerations in the design were sufficient to ensure the required precision of the Tx/Rx alignment. Otherwise, the misalignment would have led to additional losses, and reliable links would not have been possible in this regard. Whenever OSIRIS4CubeSat tracked the beacon sent by the OGS, the light seen on the ground was received uninterruptedly during the entire tracking phase, even at the lowest elevations.

The link budget could not be verified in detail during the PIXL-1 mission, as the focus of the mission was the successful data transmission. Thus, it can only be assumed that the link budget was conservatively calculated, based on the mission observations. Nevertheless, there are—besides the successful picture transmission—two indications which led to the assumption that the system performed more than sufficiently to cover considered use cases. One indication in the uplink direction was the ADC values of the 4QD, which are illustrated in Figure 8.

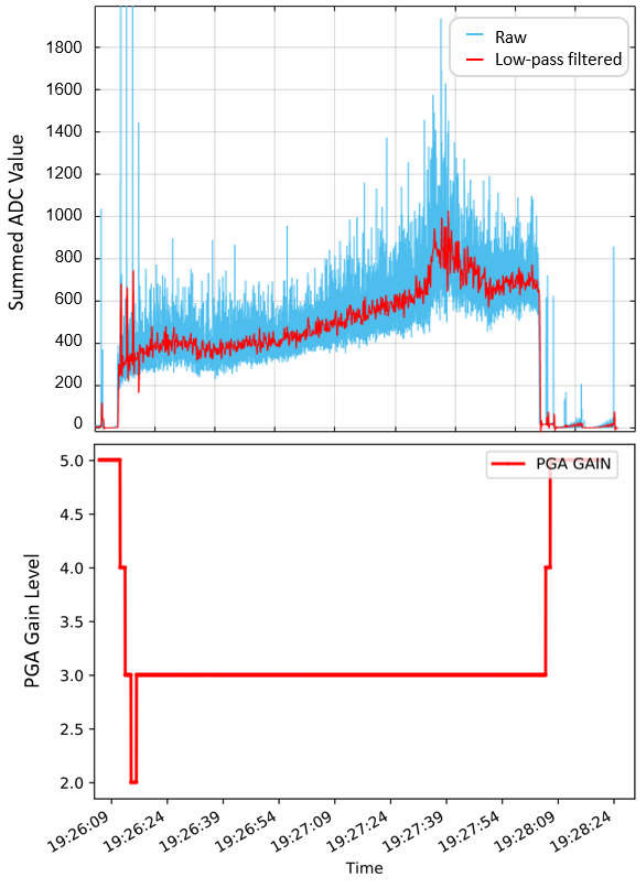

Figure 8. 4QD values and PGA gains.

The picture shows the 4QD values of a laser downlink between 20° and 42.5° elevations. OSIRIS4CubeSat was equipped with a programmable gain amplifier (PGA), which amplified the received signal based on its strength. The PGA has seven levels (0 to 6) and amplified the signal according to the level with a factor of 2^{level}. As can be seen, the PGA worked mainly with level three during this example link. This relatively low amplification of the received signal means that the received signal was strong enough that it was not necessary to use the entire range of the PGA. The seven levels were intended to cover the entire dynamic range of a flyover, including at low elevations. The highest amplification level, seven, never had to be used during the mission, even at low elevation links below 5°. This exceeded the expectations of the system's design.

To evaluate the signal integrity of the transmitter system and obtain an indication of the received power, the received data were collected by a digital oscilloscope. Figure 9 shows one example of the received signal.

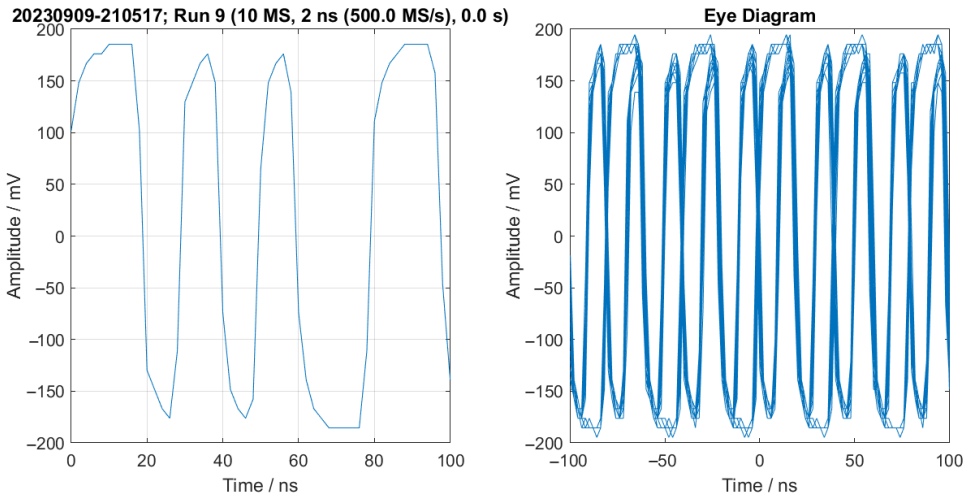

Figure 9. HPLD received signal.

The signal displayed in Figure 9 is the analog output of the OGS's receiver frontend, sampled at 500 megasamples per second (MS/s) for a link at 20° elevation. As already stated, the OGS was not equipped with an optical power meter to measure the signal strength directly. It can be seen that the receiver output level was close to 400 mV peak-to-peak, which had already saturated the receiver. To this day, OSIRIS4CubeSat operates at 60 mW, as it was seen that this reduced power was still sufficient to receive data even at elevations below 5°. The link budget considered a successful data transmission with 100 mW optical output power above 10° elevation.

The rise and fall times are optimized for 100 Mbps, and the eye diagram shows good signal integrity. In conclusion, Figure 5 illustrates the required transmission system performance from the transmitter over the channel to the receiver.

The goal of the PIXL-1 mission was the successful demonstration of the entire data transmission chain from the data generation (image capture), the transmission via laser, and the decoding on the ground. The scientific evaluation of the channel characteristics, and, with this, the link budget verification, was not a goal of the mission. These activities are covered by the successor mission QUBE, where OSIRIS4CubeSat was evolved towards the capabilities of quantum key distribution. The systems OSIRIS4CubeSat and OSIRIS4QUBE are—with regard to the classical optical channel—identical, and the results of the QUBE mission can therefore be used to verify the link budget presented in Section 3.1 [30]. These measurements were not completed at the time of writing this publication.

6. Discussion and Conclusions

The successful in-orbit demonstration verified and proved the overall payload design. In general, it can be said that the miniaturization of laser communication to serve the commercial CubeSat market is feasible. The transition to Tesat and, with this, the industrialization of the terminal emphasizes this [11].

Using the PCB as an optical bench enabled the level of miniaturization which had to be proven in this work. The optomechanical system where the optical elements were integrated into solid aluminum blocks enabled the required stiffness to reduce vibrations and thermal effects. This could already be verified during the qualification process of the terminal. The reliable connection in space also proved the selection of the optical components as reliable for the considered use case. Future concepts can be based on this development to achieve the necessary robustness in combination with high compactness.

The reliability of the control concept was proven during the final satellite mission. The stability of the tracking showed that the design of the controller and the hardware design are functional and sufficient to achieve the required precision. Stray light from the transmitter laser onto the 4QD could be mitigated by prior optical calibration of the system in orbit [24]. For future systems, this should be mitigated by hardware measures in the optical domain to prevent sensors misbehaving from stray light. Besides the tracking, it was also noticeable that the acquisition and tracking were highly dependent on the satellite's orientation. A target pointing of ±1° is easily achievable by the actuators, but the inputs of the absolute sensors must be very reliable. This results in strict requirements for the carrier platform if the system presented in this work is used. Nevertheless, this work should have evaluated the control loop development for a laser communication system, and its functionalities and abilities could be demonstrated and verified during the in-orbit mission.

The challenging design of a transmitter system generating a data signal with 100 Mbps could be verified by the signal integrity on the ground. The open eye in Figure 5 and the similarity to the characterization measurements in the lab in Figure 4 show that a receiver front end can easily distinguish a digital one from a digital zero. The open eye indicates the reception of the signal without any misinterpretation of bits. The high peak-to-peak voltage of 400 mV after the transmission from the satellite in orbit overcomes the considerations in the link budget. Even though no direct optical power measurement has been possible to this day, the results show that the system performs slightly better than assumed by the basic calculations.

CubeSats are very efficient, but their resources are nevertheless limited. Thus, synergies inside the satellite bus are a reasonable approach to save resources. The distributed software parts on the terminal itself and the SDR of the satellite demonstrate very well how free processing resources can be used. The full data processing chain demonstrated, for the first time, an operational use case on a CubeSat using laser communication.

A major property for operational use cases is interoperability, which requires standardized connections. The patented communication channel developed in this project is orientated on the CCSDS standard and can be used as an example implementation for future missions. Even though the standard is not fully published yet, the full end-to-end transmission demonstrated the usability of the O3K standard.

The goal of this work was to develop a miniaturized laser communication terminal for high data rates that serves potential operational use cases on CubeSats. With the results of the PIXL-1 mission, it can be stated that this goal was well achieved. The scientific evaluation of the propagation channel and the link budget will be carried out during successor missions.

7. Patents

The following patents were published during the course of this project:

- "Elektrisch-optischer Aufbau" (DE102016221137A1), filed on 26.04.2018, by C. Schmidt.
- "Method for data transmission from a spacecraft to ground via a free-space optical channel" (EP4256726B1 and US20230421251A1), filed on 01.12.2021, by A. Morab Vishwanath.

Author Contributions: Conceptualization, C.S.; Formal analysis, C.R., F.R., R.R., and A.M.V.; Funding acquisition, C.S.; Investigation, C.R., F.R., R.R., and A.M.V.; Methodology, B.R.; Project administration, C.S.; Software, F.R., R.R., and A.M.V.; Supervision, B.R.; Validation, B.R.;

Visualization, C.R., F.R., and A.M.V.; Writing—original draft, B.R.; Writing—review and editing, B.R. and C.S. All authors have read and agreed to the published version of the manuscript.

Funding: The authors declare that this study received funding from Tesat-Spacecom GmbH and Co. KG. The funder had the following involvement with the study: Funding the terminal development and the demonstrator mission as well as supporting with technical expertise during project reviews.

Data Availability Statement: The data presented in this study can be requested from the corresponding author and can be provided if it corresponds with the legal regulations between the researcher and the funder.

Acknowledgments: The authors would like to thank the German Space Operation Center (GSOC) team for their support in the operation of the PIXL-1 mission and all colleagues from the Optical Satellite Links (OSL) department who supported us—especially during the laser downlink campaign.

Conflicts of Interest: The authors declare that the research was conducted in the absence of any commercial or financial relationships that could be construed as a potential conflict of interest

Abbreviations

The following abbreviations are used in this manuscript:

4QD	Four-quadrant diode
ADC	Analog-to-digital converter
ADCS	Attitude determination and control system
BiROS	Bi-spectral Infrared Optical System
CAN	Controller area network
CCSDS	Consultative Committee for Space Data Systems
CLICK	CubeSat Laser Infrared Crosslink
COTS	Commercial off-the-shelf
CSP	CubeSat space protocol
CTE	Coefficient of thermal expansion
DAC	Digital-to-analog converter
DBS	Dichroic beam splitter
DC	Direct current
DLR	German Aerospace Center
DMA	Direct memory access
EDFA	Erbium-doped fiber amplifier
EDRS	European Data Rely System
FEC	Forward error correction
FOR	Field of regard
FPGA	Field programmable gate array
FSM	Fast-steering mirror
FSOC	Free-space optical communications
Gbps	Gigabit per second
GSOC	German Space Operation Center
HPLD	High-power laser diode
JTAG	Joint test action group
JPEG	Joint photographic experts group
LCT	Laser communication terminal
LEO	Low earth orbit
M1	Primary mirror
M2	Secondary mirror
Mbps	Megabit per second
MS/s	Megasamples per second
NASA	National Aeronautics and Space Administration
O3K	Optical on–off-keying

OBC	Onboard computer
OGS	Optical ground station
OSIRIS	Optical Space Infrared Downlink System
OSL	Optical Satellite Links
PAA	Point ahead angle
PAT	Pointing, acquisition, and tracking
PCB	Printed circuit board
PGA	Programmable gain amplifier
PI	Proportional–integral
PRBS	Pseudo-random bit sequence
RF	Radio frequency
RS	Reed–Solomon
Rx	Receiver
SDR	Software-defined radio
SOCRATES	Space Optical Communications Research Advanced Technology Satellite
SPI	Serial peripheral interface
SWaP	Size, weight, and power
TBIRD	Terabyte Infrared Delivery
TCXO	Temperature-compensated crystal oscillator
TEC	Thermoelectric cooler
Tesat	Tesat-Spacecom GmbH & Co. KG
TNO	Netherlands Organization for Applied Scientific Research
Tx	Transmitter
U	Unit
USART	Universal synchronous/asynchronous receiver/transmitter

References

1. Buscher, M.; Brieß, K. Investigations on the Current and Future Use of Radio Frequency Allocations for Small Satellite Operations; Universitätsverlag der TU Berlin: Berlin, Germany, 2019. https://doi.org/10.14279/depositonce-8247.
2. The European Space Agency (ESA), *EDRS Overview*, 2024. online: https://www.esa.int/Applications/Telecommunications_Integrated_Applications/EDRS/Overview (accesses 23 may 2025).
3. Brashears, T.R. Achieving ≳99% Link Uptime on a Fleet of 100G Space Laser INTER-satellite Links in LEO. In Proceedings of Volume 12877, Free-Space Laser Communications XXXVI, San Francisco, CA, USA, 30–31 January 2024. https://doi.org/10.1117/12.3005057.
4. Giggenbach, D.; Fuchs, C.; Schmidt, C.; Rödiger, B.; Gaißer, S.; Klinkner, S.; Phung, D.-H.; Chabe, J.; Courde, C.; Maurice, N.; et al. Downlink communication experiments with OSIRISv1 laser terminal onboard Flying Laptop satellite. *Appl. Opt.* **2022**, *61*, 1938–1946. https://doi.org/10.1364/AO.446771.
5. Takenaka, H.; Koyama, Y.; Akioka, M.; Kolev, D.; Iwakiri, N.; Kunimori, H.; Carrasco-Casado, A.; Munemasa, Y.; Okamoto, E.; Toyoshima, M. In-orbit verification of small optical transponder (SOTA): Evaluation of satellite-to-ground laser communication links. In Proceedings of Volume 9739, Free-Space Laser Communication and Atmospheric Propagation XXVIII, San Francisco, CA, USA, 15–16 February 2016. https://doi.org/10.1117/12.2214461.
6. Cierny, O.; Serra, P.; Kammerer, W.; Grenfell, P.; Gunnison, G.; Kusters, J.; Payne, C.; Pereira, P.D.V.; Cahoy, K.; Conklin, J.; et al. Testing of the CubeSat Laser Infrared CrosslinK (CLICK-A) Payload. In Proceedings of the Small Satellite Conference, Utah, USA, 1-6 August 2020.
7. Kammerer, W.; Grenfell, P.; Harburg, J.; Belsten, N.; Tomio, H.; Serra, P.; Cahoy, K.; Brothers, T.; Person, M.; Clark, M.; et al. CLICK-A: Optical Communication Experiments From a CubeSat Downlink Terminal. In Proceedings of the Small Satellite Conference, Utah, USA, 5-10 August 2023.
8. Plooy, J.D.; Hejderup, J.; Engelen, S.; Witvoet, G.; Herfst, R.; de Bruin, D.; Redi, S.; van Kempen, F. CubeCAT: In-Orbit Results and the Future of DTE LCT. In Proceedings of Volume 13546, Small Satellites Systems and Services Symposium (4S 2024), Palma de Mallorca, Spain, 27–31 May 2024. https://doi.org/10.1117/12.3061323.
9. Schieler, C.M.; Riesing, K.M.; Horvarth, A.J.; Bilyeu, B.C.; Chang, J.S.; Garg, A.S.; Wang, J.P.; Robinson, B.S. 200 Gbps TBIRD CubeSat Downlink: Pre-Flight Test Results. In Proceedings of the Proceedings Volume 11993, Free-Space Laser Communications XXXIV, San Francisco, CA, USA, 22–27 January 2022. https://doi.org/10.1117/12.2615321.

10. Schieler, C.; Robinson, B.; Guldner, O.; Bilyeu, B.; Garg, A.; Riesing, K.; Chang, J.; Hakimi, F.; Brown, J.; Khatri, F.; et al. NASA's Terabyte Infrared Delivery (TBIRD) Program: Large-Volume Data Transfer from LEO. In Proceedings of the Small Satellite Conference, Utah, USA, 3-8 August 2019.
11. Pimentel, P.M.; Rödiger, B.; Schmidt, C.; Fuchs, C.; Rochow, C.; Hiemstra, T.; Zager, A.; Wertz, P.; Knopp, M.T.; Lehmann, M.; et al. Cube Laser Communication Terminal (CubeLCT) state of the Art. *Acta Astronaut.* **2023**, *211*, 326–332. https://doi.org/10.1016/j.actaastro.2023.06.026.
12. DelPozzo, S.; Williams, C. *Nano/Microsatellite Market Forecast*; SpaceWorks Enterprises: Atlanta, GA, USA, 2020, https://doi.org/10.13140/RG.2.2.24280.32005.
13. Fuchs, C.; Moll, F.; Giggenbach, D.; Schmidt, C.; Keim, J.; Gaißer, S. OSIRISv1 on Flying Laptop: Measurement Results and Outlook. In Proceedings of the 2019 IEEE International Conference on Space Optical Systems and Applications (ICSOS), Portland, USA, 14–16 October 2019. https://doi.org/10.1109/ICSOS45490.2019.8978984.
14. Fuchs, C.; Schmidt, C.; Keim, J.; Moll, F.; Rödiger, B.; Lengowski, M.; Gaißer, S.; Giggenbach, D. Update on DLR's OSIRIS Program and first results of OSIRISv1 on Flying Laptop. In Proceedings of the SPIE—The International Society for Optical Engineering, San Francisco, USA, 2-7 February 2019. https://doi.org/10.1117/12.2514349.
15. Schmidt, C.; Fuchs, C. Elektrisch-optischer Aufbau, DE patent DE102016221137A1, 2018, https://patents.google.com/patent/DE102016221137A1/fr.
16. Schmidt, C. *Optische Kommunikation auf CubeSats*; Dissertation, Shaker Verlag: Aachen, Germany, 2023; ISBN 978-3-8440-9265-3.
17. Rüddenklau, R.; Rein, F.; Roubal, C.; Rödiger, B.; Schmidt, C. In-orbit demonstration of acquisition and tracking on OSIRIS4CubeSat. *Opt. Express* **2024**, *32*, 41188–41200. https://doi.org/10.1364/OE.537889.
18. Rödiger, B.; Rüddenklau, R.; Schmidt, C.; Lehmann, M. (2022) Acquisition Concept for Inter-Satellite Communication Terminals on CubeSats. In Proceedings of the Small Satellites Systems and Services—The 4S Symposium 2022, Vilamoura, Portugal, 16-20 May 2022.
19. Giggenbach, D.; Knopp, M.T.; Fuchs, C. Link budget calculation in optical LEO satellite downlinks with on/off-keying and large signal divergence: A simplified methodology. *Int. J. Satell. Commun. Netw.* **2023**, *41*, 460–476. https://doi.org/10.1002/sat.1478.
20. Andrews, L.C.; Phillips, R.L. *Laser Beam Propagation through Random Media*, 2nd ed.; SPIE Press: Bellingham, WA, USA, 2005. https://doi.org/10.1117/3.626196.
21. Moll, F.; Giggenbach, D.; Schmidt, C.; Fuchs, C. Analysis of power scintillation and fading margin in the LEO-ground downlink with the OSIRISv1 laser terminal on Flying Laptop and the DLR optical ground station Oberpfaffenhofen. In Proceedings of the Environmental Effects on Light Propagation and Adaptive Systems V 2022, Berlin, Germany, 6 September 2022. https://doi.org/10.1117/12.2647830.
22. Carrillo-Flores, A.; Giggenbach, D.; Knopp, M.; Orsucci, D.; Shrestha, A. Effects of pointing errors on intensity losses in the optical LEO uplink. In Proceedings of the SPIE 12777, International Conference on Space Optics—ICSO 2022, 127775U, Dubrovnik, Croatia, 3–7 October 2022. https://doi.org/10.1117/12.2691100.
23. Roubal, C.; Dolejsky, T.; Rödiger, B.; Rein, F.; Nonay, J.R.; Rüddenklau, R.; Papadopoulos, C.; Schmidt, C.; Moll, F. Laser Terminals on CubeSats: Developments for Telecommunications and Quantum Links. *Int. J. Satell. Commun. Netw.* **2025**, *43*, 133–146. https://doi.org/10.1002/sat.1545.
24. Rüddenklau, R.; Rein, F.; Roubal, C.; Rödiger, B.; Schmidt, C. In-orbit optical calibration for acquisition and tracking on OSIRIS4CubeSat. In Proceedings of Volume 13355, Free-Space Laser Communications XXXVII, San Francisco, USA, 28–31 January 2025. https://doi.org/10.1117/12.3039395.
25. Moll, F. *Trials and Analysis;* GOLCE: Tenerife, Spain, 2010; ISSN 2185-1484.
26. Rödiger, B.; Rüddenklau, R.; Vishwanath, A.M.; Roubal, C.; Moll, F.; Fuchs, C. Verification of laser communication terminals for CubeSats as preparation for missions PIXL-1 and QUBE under atmospheric conditions. In Proceedings of the 75th International Astronautical Congress, IAC 2024, Milan, Italy, 14–18 October 2024; ISSN 0074-1795. https://doi.org/10.52202/078363-0093.
27. Consultative Committee for Space Data Systems (CCSDS): Optical Communications Coding and Synchronization, Blue Book, CCSDS 142.0-B-1, Washington, DC, USA, CCSDS Secretariat, August 2019, https://ccsds.org/Pubs/142x0b1.pdf
28. A. Morab Vishwanath, Method for data transmission from a spacecraft to ground via a free space optical channel, EU patent EP4256726B1, US patent US20230421251A1, https://data.epo.org/publication-server/rest/v1.2/patents/EP4256726NWB1/document.pdf.

29. Rödiger, B.; Schmidt, C. In-orbit demonstration of the world's smallest laser communication terminal—OSIRIS4CubeSat/CubeLCT. In Proceedings of Volume 13546, Small Satellites Systems and Services Symposium (4S 2024), Palma de Mallorca, Spain, 27–31 May 2024. https://doi.org/10.1117/12.3060897.
30. Knips, L.; Auer, M.; Baliuka, A.; Bayraktar, O.; Freiwang, P.; Grünefeld, M.; Haber, R.; Lemke, N.; Marquardt, C.; Moll, F.; et al. QUBE—Towards Quantum Key Distribution with Small Satellites; Quantum: Boston, MA, USA, 2022. https://doi.org/10.1364/QUANTUM.2022.QTh3A.6.

Disclaimer/Publisher's Note: The statements, opinions and data contained in all publications are solely those of the individual author(s) and contributor(s) and not of MDPI and/or the editor(s). MDPI and/or the editor(s) disclaim responsibility for any injury to people or property resulting from any ideas, methods, instructions or products referred to in the content.